RSC Advances

REVIEW

View Article Online
View Journal | View Issue

Cite this: *RSC Adv.*, 2024, **14**, 23322

On the role of disjoining pressure in nanofluid-assisted enhanced oil recovery: a mini-review

Baoliang Peng, †[a] Han Gao, †[b] Qiying Liu,[b] Ping Yi,[c] Yingying Li,[a] Weidong Liu*[a] and Ye Xu *[b]

Nanofluid application in enhanced oil recovery (EOR) recently emerged and garnered significant attention within the field. Nanofluids possess unique properties of reducing oil–water interfacial tension, stabilizing emulsions, altering rock surface wettability, and enhancing disjoining pressure between crude oil and rock surfaces, therefore have potential for the oil recovery process. This review provides an in-depth exploration of various aspects related to nanofluids in EOR. Different types of nanofluids are presented with their preparation methods and representative properties. More importantly, the disjoining pressure, a key physical concept in nanofluid-assisted EOR, is introduced and discussed in terms of the mechanism of oil displacement and measurement methods. Further understanding the role of disjoining pressure in nanofluid-assisted oil displacement is necessary for the development and application of effective nanofluids for EOR.

Received 24th April 2024
Accepted 14th July 2024

DOI: 10.1039/d4ra03036b

rsc.li/rsc-advances

1. Introduction

In the petroleum industry, enhanced oil recovery (EOR) stands as a pivotal and indispensable phase within the oil production process, designed to extract crude oil from reservoirs that would otherwise remain unrecoverable.[1–4] EOR is defined as the injection of a special solution/gas into the reservoir so that crude oil trapped inside can be driven out of the pore or gap.[5] Four prevalent EOR techniques have emerged, including chemical injection, gas injection, microbial methods, and thermal processes.[6–9] Briefly, chemical injection EOR is a process that injects selected chemicals into the reservoir, thereby altering the reservoir's physicochemical properties.[10] Meanwhile, gas injection EOR mainly uses CO_2 as the primary agent to displace oil.[11] Microbial EOR, on the other hand, relies on the utilization of microorganisms and their metabolic byproducts to effectively mobilize oil from reservoirs.[12] Thermal

[a]*Key Laboratory of Oilfield Chemistry, CNPC, Research Institute of Petroleum Exploration & Development (RIPED), PetroChina, Beijing 100083, China. E-mail: lwd69@petrochina.com.cn*

[b]*School of Mechanical Engineering and Automation, Beihang University, Beijing 100191, China. E-mail: ye.xu@buaa.edu.cn*

[c]*National Engineering Laboratory for Exploration and Development of Low Permeability Oil and Gas Fields, Oil and Gas Technology Research Institute, PetroChina Changqing Oilfield Company, Xi'an 710018, China*

† These authors contributed equally to this work and should be considered co-first authors.

Baoliang Peng

Baoliang Peng is a senior engineer at the Research Institute of Petroleum Exploration and Development (RIPED), PetroChina. In 2007, he started his graduate study, and joined a dual-degree doctoral program between the University of Waterloo and East China University of Science and Technology (ECUST). He earned his PhD in 2014. His research interests focus on fundamental mechanism and chemical materials for enhanced oil recovery applications.

Han Gao

Han Gao is a PhD candidate in the School of Mechanical Engineering and Automation at Beihang University, China. His research focuses on the dynamics and manipulation of nanoparticles.

processes can decrease oil viscosity or change the rock's wettability by introducing heat into a light oil reservoir.[6]

Nanofluid EOR, a special chemical EOR method, has been proposed and attracted significant attention within the field recently.[13–17] A nanofluid, in brief, is a suspension comprising solid nanoparticles that are uniformly dispersed within a solvent medium.[18,19] It has been reported that nanofluids show many advantageous properties inherent in the context of EOR, including high stability, low erosion, and friction coefficients, and good lubrication.[20–23] Furthermore, the distinctive characteristics exhibited by the contained nanoparticles, including their small size and high surface-to-volume ratio, significantly contribute to the reduction of oil–water interfacial tension and the alteration of rock wettability.[24]

Due to the potential advantages offered by nanofluids in EOR, researchers have dedicated efforts to investigating the mechanisms behind oil recovery through nanofluids. Prior studies have identified four primary aspects of the EOR mechanism involving nanofluids: (1) reduction of oil–water interfacial tension, (2) enhanced stability of oil–water emulsions, (3) alteration of rock wettability, and (4) increase of disjoining pressure between oil and rock surface. The reduction of the oil–water interfacial tension is the result of a single or multi-layer film of nanoparticles that are strongly adsorbed on the oil–water interface.[25–27] In addition, these solid particles create an interconnected network that envelops the oil–water emulsions, giving rise to the enhanced stability and resistance to rupture.[28,29] Moreover, nanoparticles can attach to the surface of rocks, generating diverse structures that effectively transform the wettability of the rock. The simulation proved that the water-wet state has a higher oil recovery than the oil-wet state for oil-saturated pores and wettability effects can help oil to detach from the pore walls for oil-unsaturated pores.[30] More importantly, recent studies found that the disjoining pressure, generated by the orderly accumulation of nanoparticles at the oil–water–solid three-phase interface, can effectively separate the oil from the rock surface.[13,31–33] While the reduced oil–water interfacial tension and altered wettability due to strong adsorption of nanoparticles to the oil–water interface or the rock surface are well understood, the systematic assessment of the role of disjoining pressures in EOR is still lacking.

Ye Xu

Ye Xu is a professor of soft materials and mechanics in the School of Mechanical Engineering and Automation at Beihang University, China. He earned his PhD degree in 2012 from Yale University. His current research interests include soft matter physics and mechanics, flexible micro-nanomaterials and structures, and microfluidic devices.

This review focuses on the role of disjoining pressure in the presence of nanofluids and its consequential impact on the EOR processes. The review is structured in the following way. The first part introduces different types of nanofluids and their preparation methods. Key properties of those nanofluids, including suspension stability, thermophysical properties, and flow properties, are also presented. In the second part, the disjoining pressure is defined and formulated in terms of its three components including van der Waals force, electrostatic force, and structural disjoining pressure, followed by a discussion on the mechanism of the disjoining pressure in EOR. The third part reviews the measurement methods in the study of disjoining pressures, including the direct measurement of and the indirect method through the liquid film thickness. Finally, the prospects of the nanofluids in EOR are discussed, therefore offering a forward-looking perspective on this topic.

2. Nanofluids used in EOR

2.1 Preparation methods of nanofluids

Nanofluids are defined as suspensions obtained through the even dispersion of nano-sized solid particles in liquid media such as water, ethylene glycol, and oil. The liquid component is immiscible with solid particles, and the size of solid particles is in the range of 1–100 nm. As a major component of nanofluids, the appropriate selection of nanoparticles is crucial in improving the efficacy of EOR.[19,55,56] Generally, nanoparticles can be categorized into four groups: metals, metal oxides, non-metallic oxides, and carbon nanotubes based on their chemical composition, as detailed in Table 1. There are also some nanoparticles not included in this category, such as copper quantum dot/polyacrylamide composite nanospheres,[57] MoS_2,[29] Kaolinite-based Janus nanosheets,[58] 2D Janus polymer nanosheets.[59] Currently, non-metallic oxide nanoparticles and metal oxide nanoparticles are widely applied in EOR, primarily due to their capacity to alter the wettability of rocks or reduce oil–water interfacial tension.[46,50,51] Particularly, as a principal rock component, SiO_2 nanoparticles are commonly used for EOR application.[51,60–64] Chaturvedi *et al.* prepared a stable SiO_2 nanofluid that interacts with polymer chains and creates a steric barrier to improve CO_2 absorption for oilfield applications.[65] Moreover, the SiO_2 nanofluid could also improve CO_2 flow and reduce formation damage in porous media for carbon utilization.[66]

There are two main preparation methods for nanofluids, namely the one-step method and the two-step method.[67–70] In the one-step method, nanoparticles are generated and uniformly dispersed into the base liquid within the same preparation process.[71] In the two-step method, by contrast, nanoparticles are first prepared, mostly using the solution-based method, and then dispersed in a certain proportion into the base fluid.[72] To ensure uniform dispersion of nanoparticles, techniques including ultrasonic vibration, magnetic stirrer, and the addition of dispersant to the fluid are commonly employed.[73,74] Nanofluids prepared by the one-step method usually exhibit high purity and good stability, which determine whether the nanoparticles can function effectively, especially in

Table 1 Nanoparticles in nanofluids and improvement in EOR

Categories	Examples	Advantages
Metals	Cu,[34,35] Ag,[36] Au,[37,38] Fe,[39] *etc.*	Electrical conductivity and chemical catalysis
Metal oxides	Al_2O_3,[40,41] CuO,[42,43] TiO_2,[44,45] ZrO_2,[46,47] *etc.*	Alter the wettability of carbonate reservoir rocks[46]
Non-metallic oxides	SiO_2,[48] $CaCO_3$,[49] *etc.*	Reducing oil–water interfacial tension in light reservoirs[50] and non-polluting as the main component of rock[51]
Carbon nanotubes	MWCNT,[52] DWCNT[53]	Reducing the viscosity of crude oil[54]

nanofluid flooding systems. For example, Aberoumand *et al.*[75] used the one-step method to prepare a Cu nanofluid, composed of high-purity copper nanoparticles and engine oil without surfactant and exhibiting good stability at room temperature. Despite the advantage of avoiding the oxidation of nanoparticles and the separate processes like drying, transportation, storage, and additional dispersion of nanoparticles, the one-step process entails complexity and necessitates substantial equipment investment, rendering it unsuitable for large-scale production endeavors.[75,76] On the other hand, the two-step preparation process is simple, cost-effective, and therefore feasible for large-scale production. Nevertheless, nanofluids produced through the two-step method tend to be relatively unstable, prone to coalescence and precipitation, and therefore often require stirring or the inclusion of dispersants.[39,76]

2.2 Properties of nanofluids

Compared to the general fluid without nanoparticles, nanofluids exhibit special characteristics of thermophysical and flow properties.[77] The addition of nanoparticles can improve the thermal conductivity of simple fluids such as glycol and water. For example, Xing *et al.*[78] found that the thermal conductivity of carbon nanotube nanofluid was higher than that of base fluid deionized water, and increased with the increase of the nanoparticle concentration and temperature. As for the flow property, it is well observed that the nanofluid shows higher viscosity than that of the base fluid, and the viscosity increases with the concentration of nanoparticles.[79] The higher viscosity of nanofluids can improve the mobility ratio.[80] For a high viscosity ratio, displacement occurred in the form of capillary fingers at low capillary numbers while the displacement gradually became stable at high capillary.[81] Interestingly, even in cases where nanofluid viscosity rises with concentration, Sefiane *et al.*[82] found that aluminum nanofluids exhibit greater spreading capability across solid surfaces compared to ordinary fluids, even though the viscosity of the nanofluids is higher.

In addition to the general ones discussed above, the properties of nanofluids particularly important for EOR are the ability to alter the interfacial tension (IFT) of oil–water and the wettability of rock. Joonaki and Ghanaatian[83] studied the effect of three nanofluids (Al_2O_3, SiO_2, Fe_2O_3) on IFT, revealing that increasing the nanoparticles concentration led to reduced IFT and a shift towards a more neutrally wetted solid surface. Notably, SiO_2 was more efficient in reducing IFT between oil and water. Tohidi *et al.*[84] proved that silica Janus nanoparticles can increase the viscosity of water phase and reduce the IFT using molecular dynamics simulation. Furthermore, a hydrophilic SiO_2 nanofluid displayed the ability to enhance the performance of anionic surfactant in reducing IFT.[85] Besides, Moradi *et al.*[86] highlighted that SiO_2 nanofluid can induce alterations in the wettability of carbonate rock by adsorbing it onto its surface. Particularly significant wettability changes were observed when the proportion of SiO_2 nanoparticles was elevated.[87] Wettability alteration can also be estimated using simulation methods. Boampong *et al.*[88] developed a model that showed oil adsorption was still possible, even when the oil–brine and the rock–brine interfaces had the same polarity of zeta-potentials in a low-salinity water flooding system. Therefore, the wettability alteration is not related only to the polarities of the interface zeta-potentials, but also to the magnitude of the zeta-potentials.

Furthermore, the addition of surfactants, such as anionic sodium dodecyl sulfate (SDS)[89] and cationic hexadecyltrimethylammonium bromide,[90] nonionic pentaethylene glycol monododecyl ether,[91] enhancing the stability of nanofluid can also promote the oil recovery. Kumar *et al.*[92] found that the synergy between SDS and SiO_2 nanofluid subdued surfactant adsorption in both unconsolidated and consolidated porous media even at high salinity. Besides, Chaturvedi *et al.*[93] added SDS into SiO_2 nanofluid leading to an improvement in the fluid stability by reducing salt-induced nanoparticles agglomeration. The displacement results also showed that the surfactant used in the SiO_2 nanofluid for oil recovery applications provides better results than sole silica nanofluid at high temperatures and salinity.

Except for bare SiO_2 nanoparticles, other nanoparticles such as bare ZrO_2, functionalized MoS_2, or grafted SiO_2 nanoparticles were also reported to be used in EOR. Karimi *et al.*[46] prepared a ZrO_2 nanofluid that could alter the wettability of a carbonate reservoir rock from strongly oil-wet to a strongly water-wet condition. Moreover, the imbibition of ZrO_2 nanofluid into core plugs which could quickly recover oil. Functionalized nanofluid also be used in EOR. Liang *et al.*[29] improved the dynamic stability of MoS_2 nanoparticles functionalized by octadecyl amine molecules. The prepared nanofluid could reduce IFT and emulsify crude oil to a micro size which was better for EOR. In addition to being directly used as a displacement agent, there are also many reports using nanoparticle grafting other materials for EOR. Pillai *et al.*[94] found that adding lysine-grafted SiO_2 nanoparticles into surfactant could also

reduce IFT to the ultralow range and improve the stability of emulsions. Corredor *et al.*[95] reported that the fabricated nanopolymer sols (polyacrylamide-grafted SiO_2) exhibited lower IFT and the ability to alter the wettability of the substrate from oil-wet to intermediate-wet. Furthermore, the addition of the nanopolymer into hydrolyzed polyacrylamide solution could improve the solution's thickening behavior at all salinities, and increase the oil recovery of the polymer solution.

The addition of nanoparticles to assist in flooding control is also being considered. Saw *et al.*[96] found that the synergistic effects of reducing IFT between low-salinity water and SiO_2 nanoparticles can increase oil recovery significantly. In nano emulsion flooding systems, adding nanoparticles could increase droplet stability[80] and ionic strength,[97] which is also effective in EOR.

3. Disjoining pressure

3.1 Definition of disjoining pressure

Disjoining pressure is a thermodynamic concept proposed to describe the pressure difference between the inside and outside of a thin liquid film confined between two surfaces. This phenomenon arises due to the interaction forces at the molecular level and can influence the stability and behavior of liquid films in various contexts, including colloid science, wetting, and spreading phenomena,[98,99] and also in EOR applications.[26,100]

In the surface physics framework, disjoining pressure is defined as the derivative of energy as a function of the film thickness for a liquid film confined between two surfaces, either attractive or repulsive. For two flat and parallel surfaces, the disjoining pressure can be calculated as the derivative of the Gibbs energy per unit area.

Considering the intermolecular interactions, the disjoining pressure (Π) comes from three main components.[14]

$$\Pi = \Pi_m + \Pi_e + \Pi_s \quad (1)$$

where Π_m, Π_e, Π_s indicate van der Waals force, electrostatic force, and structural disjoining pressure, respectively.

The van der Waals force (Π_m) is given by

$$\Pi_m = -\frac{A_H}{6\pi h^3} \quad (2)$$

where h is the thickness of the film and A_H is the Hamaker constant determined by the three-phase dielectric constant, which is generally at the order of 10^{-19} J for a strongly hydrophilic oil–water–solid system.[101] Π_m is caused by intermolecular interactions and is a long-range attractive force, which is essential for microscale droplet spreading and film stability.

The electrostatic force (Π_e) can be written as

$$\Pi_e = \frac{\varepsilon\varepsilon_0\left(\frac{\pi kT}{ze}\right)}{2h^2} \quad (3)$$

where ε, ε_0 represent dielectric constants of vacuum and water respectively, k is the Boltzmann constant, T is the temperature, z is the zeta potential, and e is the electronic charge. Π_e can be a long-range repulsive force or attractive force, which depends on the zeta potential.[102] For example, the brine/oil zeta potential displays negative,[103] while the brine/calcite zeta potential is positive.[104]

The structural disjoining pressure (Π_s) is analytically expressed as

$$\Pi_s(h) = \begin{cases} -P, & 0 < h < d \\ \Pi_0 \cos(\omega h + \varphi_2)e^{-\kappa h} + \Pi_1 e^{-\delta(h-d)}, & h > d \end{cases} \quad (4)$$

where Π_0, Π_1, ω, φ_2, κ are coefficients related to the volume fraction of nanoparticles, δ is the short-range decay coefficient, d is the diameter of nanoparticles, and P is the volume osmotic pressure, whose expression is

$$P = \rho kT\left[\frac{1+\varphi+\varphi^2-\varphi^3}{(1-\varphi)^3}\right] \quad (5)$$

where ρ denotes the particle concentration. As the volume fraction φ of nanoparticles increases, the structural disjoining pressure and osmotic pressure also increase. Π_s is a short-range repulsive force and it plays an important role for the properties of the solid–liquid interface.[100]

3.2 Effects of disjoining pressure in EOR

In the context of EOR, disjoining pressure is used to understand the interaction between oil, water, and solid surfaces within porous rock. When nanoparticles accumulate orderly at the oil–water–solid interface, they can create a pressure difference within the confined spaces of the rock's pores. This disjoining pressure can help detach oil from the rock surface, aiding in the recovery of oil during EOR processes.[25,26]

Within nanofluid flooding systems, structural disjoining pressure as a component of disjoining pressure described in 3.1 is dominating compared to the other two components. The reason is that the structural disjoining pressure has a greater range and magnitude than the van der Waals and electrostatic forces in terms of long-range properties. The foremost source of structural disjoining pressure arises from the organized arrangement of nanoparticles. Thus, the structural disjoining pressure is related to the volume fraction of nanoparticles, and increasing volume fractions lead to larger structural disjoining pressures and thus enhanced spreading.[82] Recently, Shane[32] used the microchip to visualize the EOR process induced by structural disjoining pressure in a porous environment and proved the disjoining pressure, not the IFT reduction enhanced oil recovery using high-volume fraction nanofluids. Under the combined effect of Brownian motion and electrostatic repulsion between particles, nanoparticles dispersed in water accumulate orderly and then form a gradually advancing wedge-shaped film at the three-phase interface (oil–nanofluid–substrate) as shown in Fig. 1(a).[100] Further observations reveal that the structural disjoining pressure was perpendicular to the front oil–water interface and attenuated exponentially with the film thickness.[100,107] The attenuation factor and the oscillation period were equal to the effective diameter of the nanoparticles. As a result, the structural disjoining pressure at the front of the wedge film was higher than that near the body of the fluids.

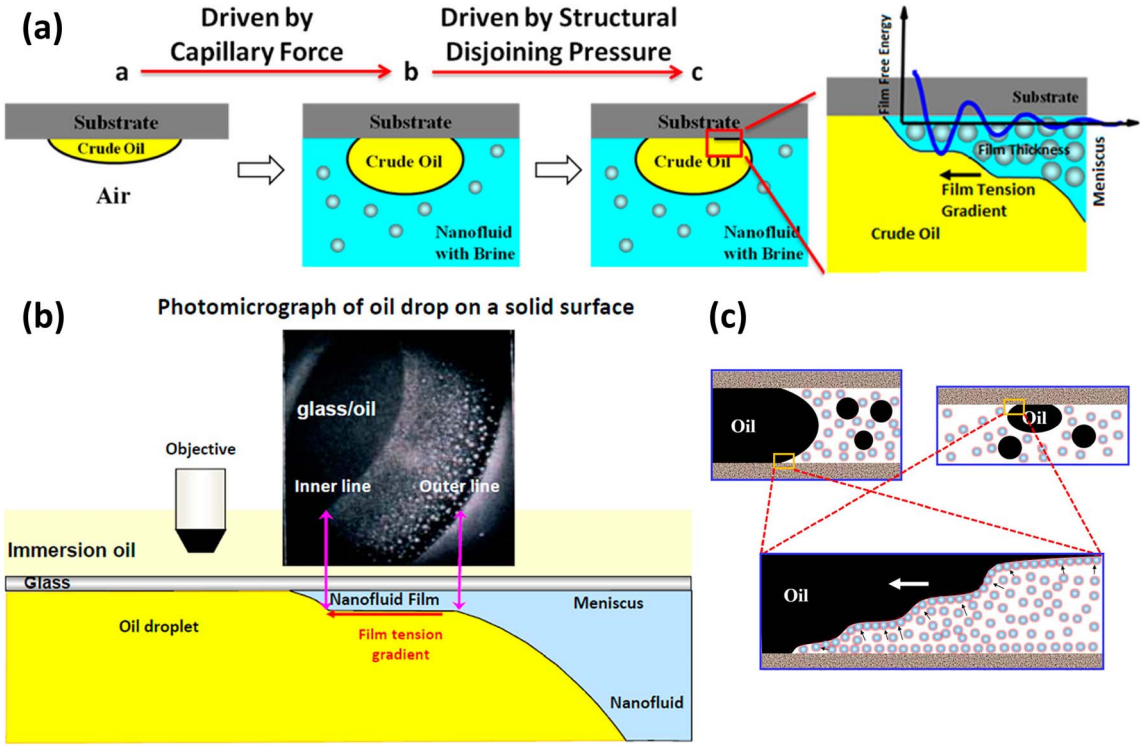

Fig. 1 (a) Forces operating at the three-phase contact line when introducing nanofluids. Reprinted with permission from (ref. 100). Copyright 2014 American Chemical Society. (b) Photomicrograph taken by reflected-light interferometry depicting the nanofluids' structural disjoining pressure in the nanofluids film region. Reprinted with permission from (ref. 105). Copyright 2012 American Chemical Society. (c) The oil displacement mechanism of nanofluids in rock pores. Reprinted with permission from (ref. 106). Copyright 2018 American Chemical Society.

Concurrently, as the structural disjoining pressure increases, the tension at the vertex of the wedge-shaped film rises gradually.

The effect of the structural disjoining pressure for the oil displacement in EOR is usually manifested in the contraction of the contact line of oil drops, which strips the crude oil from the rock surface. Kondiparty *et al.*[105] observed two distinct contact lines during the separation of oil droplets from a solid silica surface in the presence of a nanofluid (Fig. 1(b)). The outer line is the macroscopic three-phase contact line, and the inner line corresponds to the advancing nanofluid film driven by structural disjoining pressure. The dynamics of the inner contact line depend on the combination of the nanoparticle formulation, contact angle, and capillary pressure.[108] As for flooding in rock, porous rock can be regarded as a network structure composed of capillaries of different sizes. As shown in Fig. 1(c), due to Brownian motion and electrostatic force (described in Fig. 1(a)), whether the oil droplets are in the pipeline or on the wall, nanoparticles accumulate in the three-phase region.[106] The inducing structural disjoining pressure promotes the detaching of the oil droplets, thus enhancing the efficacy of oil displacement.

3.3 Measurement of disjoining pressure: direct and indirect methods

3.3.1 Direct methods. A common way to measure the disjoining pressure is a variant of a Mysels cell proposed by Bergeron.[109] As shown in Fig. 2(a), a porous glass with a micro hole in the center is welt with a capillary tube (radius r), and which other side is placed out of a chamber. The pressure of the air in the chamber controlled by a syringe pump is high compared to the pressure in the cell. Thus, a film will form in the hole when liquid is injected from the side tube, and the liquid will keep a height (h), because of the pressure difference internal and external of the chamber. Once the system is in the state of equilibrium, the disjoining pressure (Π) is

$$\Pi = P_g - P_r + \frac{2\gamma_{lv}}{r} - \rho g h \quad (6)$$

where γ_{lv} is the surface tension, ρ is the density of liquid. $P_g - P_r$ can be measured by a pressure transducer.

There are also some improved methods based on Mysels cells to measure disjoining pressure for specific liquid film systems. Dimitrova *et al.*[110,111] replaced the chamber with an open container, and the capillary side welt with a glass tube that the other side is connected with the pressure controller (Fig. 2(b)). This setup can avoid the touch between a precise pressure transducer and the organic liquid as oil phase when investigating both foam and emulsion films. It also solves the practical difficulties of applying pressure jumps on the two sides of the chamber.

In addition to the conventional methods mentioned above, a new method based on microfluid channels to measure disjoining pressure is proposed by Zou *et al.*[112] As shown in

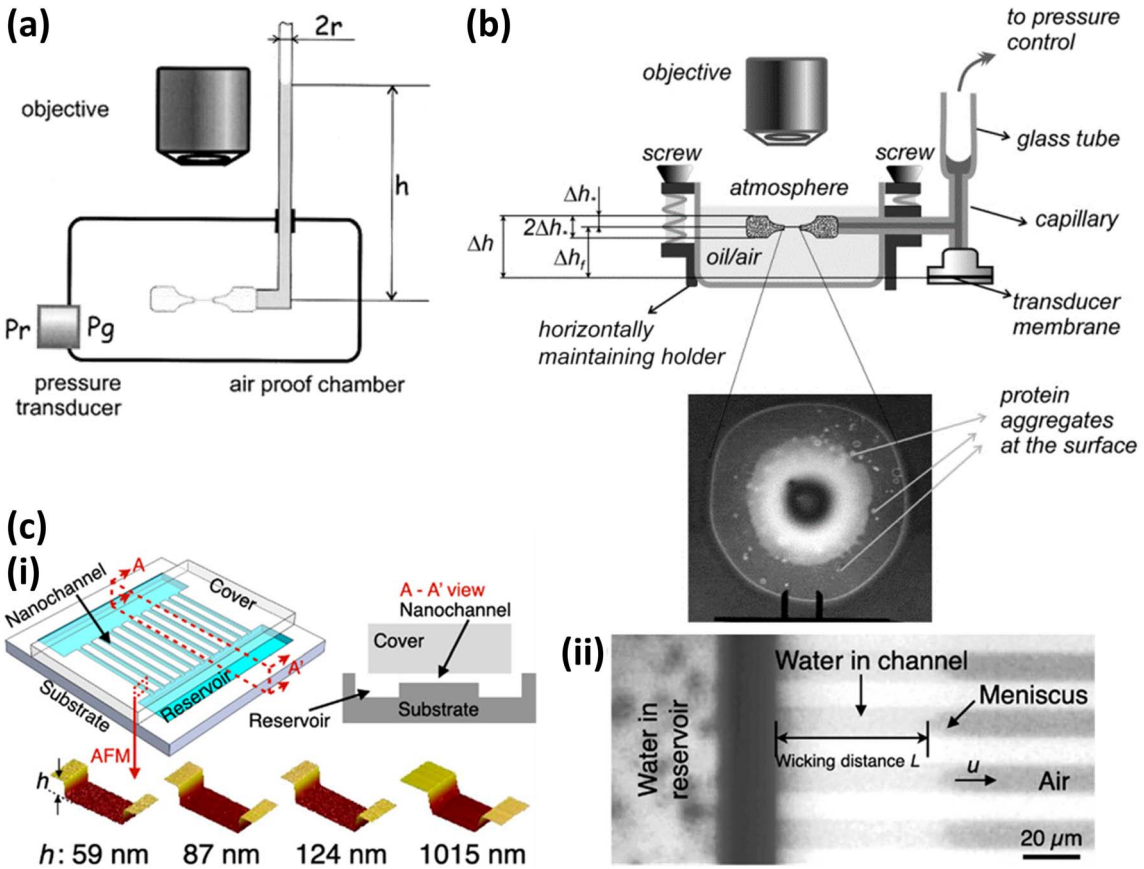

Fig. 2 Experimental setups for measuring the disjoining pressure. (a) Setup proposed by Bergeron. Reprinted with permission from (ref. 110). Copyright 2001 American Chemical Society. (b) Setup to measure disjoining pressure and thickness of film. Reprinted with permission from (ref. 111). Copyright 2004 Elsevier. (c) (i) Nanochannels with different depth and reservoirs. (ii) Wicking experiments of water. Reprinted with permission from (ref. 112). Copyright 2021 American Chemical Society.

Fig. 2(c), a silicon wafer is etched to form several parallel nanochannels whose length and width are 2 cm and 10 μm, and two deeper reservoirs connect with these channels. When one reservoir is fulfilled with water, the water will be sucked into these nanochannels because of capillary pressure. Finally, the disjoining pressure is calculated using the wicking distance, contact angle measured by image analysis, and other constant parameters including dynamic viscosity and surface tension of water, channel's height, and width. This method can simplify device requirements, such as precise pressure transducer, in comparison to using Mysels cells. In addition, the depth of the microchannel, that is, the thickness of the formed film, can be customized by etching, so that the disjoining pressure corresponding to different film thickens can be measured.

3.3.2 Indirect methods: the measurement of liquid film thickness. An indirect way to characterize the disjoining pressure is to measure the thickness of the film, which is closely related to the disjoining pressure according to the definition. During the measurement of film thickness, the formation process of the film can be characterized by the change in the thickness of the nanoparticle layers. A common Scheludko interferometric method was applied to measure the thickness of emulsion films described in many works.[110,111,113,114] While a monochromatic light reflects from the film, an interferometric image can be captured (Fig. 2(b)). Thus, the film thickness is calculated from the following relation

$$h = \frac{\lambda}{2\pi n}\left(k\pi + \arcsin\sqrt{\frac{I - I_{\min}}{I_{\max} - I_{\min}}}\right) \quad (7)$$

where I is the intensity of the reflected light, $I_{\max}$ and $I_{\min}$ are the maximal and minimal intensity of the reflected light, respectively, $k = 0, 1, \ldots$ is the order of the interference maximum, λ is the wavelength of the incident light, and n is the refractive index of the liquid film. For greater precision, a photomultiplier tube is employed to determine the intensity of the reflected light.[110] Except for forming in a cell, the film also forms near the three-phase contact line of a drop on a solid surface. In this situation, to measure values of the film thickness, which is directly related to the number of particle layers on a solid surface, Nikolov *et al.*[115] used the combined differential and commonly reflected light interferometric method to measure the film thickness of stacked nanoparticles (Fig. 3(a)). To achieve that, a specially designed glass cell eliminating light reflection from the solid substrate is combined with a differential interference microscope to observe nanoparticle self-structuring, the film thickness measured in this way can reach tens of nanometers.

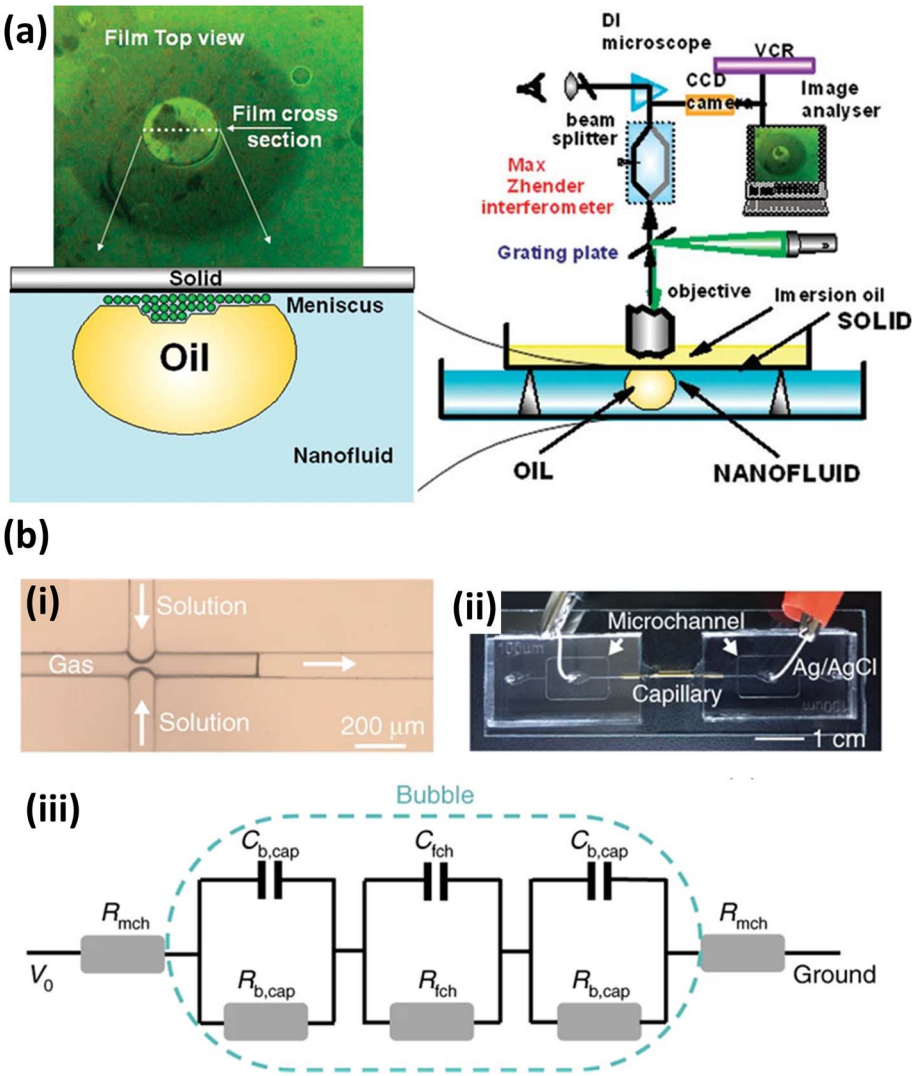

Fig. 3 (a) Observation of nanoparticle self-structuring. Reprinted with permission from (ref. 115). Copyright 2010 American Chemical Society. (b) Bubble-based film nanofluidic for film thickness measurement. (i) A snapshot of bubble formation. (ii) Picture of setup. (iii) An equivalent circuit of the system. Reprinted with permission from (ref. 116). Copyright 2020 Springer Nature.

Different from the common Scheludko interferometric method using optical filtering, a new method to produce monochromatic interferograms or images is proposed. Karakashev *et al.*[117] used a CCD high-speed camera to record the interferometric images of the whole transient films. The acquired images are then postprocessed using digital filtration techniques to generate monochromatic interferograms. In this way, different digital filters with different wavelengths to obtain the monochromatic interferograms can be provided.

In contrast to traditional optical measurements, electrical methods have also proven to be useful for measuring film thickness. Ma *et al.*[116] proposed a method that measures the film conductance to calculate the film thickness based on the derived relation between the film thickness and conductance (Fig. 3(b)). In their measurement method, a liquid film nanochannel was constructed by inserting a gas bubble in a glass capillary, and the film thickness was calculated by measuring the resistance within the channel (Fig. 3(iii)). In contrast to the previous interferometric methods, this method requires less complex optical imaging equipment. However, this method can only measure the average film thickness of the system, while the interferometric method can observe the global and local changes in film thickness in real-time.

4. Conclusion and future prospects

Oil displacement is a complex process, especially when nanofluids are used as agents. Through the extensive review of the literature related to nanofluids and disjoining pressure, we can summarize the following findings on this topic:

(1) The integration of nanoparticles in nanofluids has demonstrated a remarkable ability to alter the oil–water interfacial tension and rock surface wettability. These changes are

pivotal in enhancing the efficiency of oil recovery processes by improving the mobility and extraction of trapped crude oil.

(2) The concept of disjoining pressure, generated by the orderly self-assembly of nanoparticles at the oil–water–solid interface, is crucial in the nanofluid-assisted EOR. This pressure helps in detaching crude oil from rock surfaces, thereby significantly enhancing the oil displacement efficiency. Understanding the dynamics of disjoining pressure can lead to more effective EOR strategies.

(3) The primary research focus on nanofluid-assisted EOR is on identifying and developing more efficient nanoparticles that can optimize the flooding effect in EOR. This involves exploring different types of nanoparticles and their unique properties to determine the most effective combinations for oil recovery.

Despite the research progress survey in this review, there are still more work need to be done to further understand the crucial role of disjoining pressure in the nanofluid-assisted EOR. Particularly, it is imperative to delve deeper into the mechanisms of oil displacement facilitated by nanofluids beyond the identification of efficient nanoparticles. A comprehensive understanding of how disjoining pressure and other factors interact during the EOR process will be crucial for developing more effective applications. While indirect observations have provided valuable insights into the behavior of nanoparticles, there is a significant gap in the direct experimental observation of nanoparticle accumulation processes and the precise measurement of disjoining pressure in the three-phase region. Future research should aim to develop advanced experimental methods for direct observation and measurement. Additionally, theoretical and simulation studies should continue to evolve, providing deeper insights into the underlying mechanisms and guiding the practical application of nanofluids in EOR.

Data availability

No primary research results, software or code have been included and no new data were generated or analysed as part of this review.

Author contributions

Baoliang Peng: conceptualization, writing – original draft, supervision, funding acquisition. Han Gao: writing – original draft, writing – review & editing. Qiying Liu: writing – original draft, investigation. Ping Yi: supervision, funding acquisition. Yingying Li: supervision. Weidong Liu: resources, supervision. Ye Xu: resources, writing – review & editing, supervision, funding acquisition.

Conflicts of interest

There are no conflicts to declare.

Acknowledgements

This work was supported by the National Natural Science Foundation of China (NSFC 22008263, 11674019, and 12072010), PetroChina Basic Research and Strategic Reserve Technology Research Fund Project (2019D-500807), the Scientific Research and Technology Development Project of RIPED, PetroChina (YGJ2019-11-01), and Fundamental Research Funds for the Central Universities (YWF-22-K-101).

References

1 V. Alvarado and E. Manrique, *Energies*, 2010, **3**, 1529–1575.
2 J. Wang, L. Yu and L. X. Huang, *Pet. Sci. Technol.*, 2011, **29**, 1504–1511.
3 F. S. Zhang, J. Ouyang, X. T. Ma, H. B. Zhang, D. W. Wang and X. F. Feng, *Chem. Technol. Fuels Oils*, 2012, **48**, 202–207.
4 W. T. Zhang, Z. F. Ning, B. Zhang, Q. Wang, Z. L. Cheng, L. Huang, R. R. Qi and X. T. Shang, *J. Pet. Sci. Eng.*, 2019, **180**, 485–494.
5 G. Cheraghian and S. S. K. Nezhad, *Pet. Sci. Technol.*, 2016, **34**, 1397–1405.
6 M. Atilhan and S. Aparicio, *J. Pet. Sci. Eng.*, 2021, **205**, 108746.
7 L. Zhang, T. Petit, Y. Lu, B. E. Kratochvil, K. E. Peyer, R. Pei, J. Lou and B. J. Nelson, *ACS Nano*, 2010, **4**, 6228–6234.
8 N. Lashari and T. Ganat, *Chin. J. Chem. Eng.*, 2020, **28**, 1995–2009.
9 A. J. Scott, L. Romero-Zeron and A. Penlidis, *Processes*, 2020, **8**, 361.
10 M. Madani, G. Zargar, M. A. Takassi, A. Daryasafar, D. A. Wood and Z. Zhang, *Fuel*, 2019, **238**, 186–197.
11 Y. Lu, Y. L. Zhu, Z. H. Xu and Q. X. Liu, *Tenside, Surfactants, Deterg.*, 2019, **56**, 407–416.
12 Q. F. Cui, S. S. Sun, Y. J. Luo, L. Yu and Z. Z. Zhang, *Pet. Sci. Technol.*, 2017, **35**, 2044–2050.
13 E. Jafarbeigi, A. Mohammadidoust and B. Ranjbar, *Pet. Sci. Technol.*, 2022, **40**, 1811–1828.
14 A. O. Gbadamosi, R. Junin, M. A. Manan, N. Yekeen, A. Agi and J. O. Oseh, *J. Ind. Eng. Chem.*, 2018, **66**, 1–19.
15 S. A. C. Natalya, G. T. M. Kadja, N. J. Azhari, M. Khalil and A. T. N. Fajar, *Flatchem*, 2022, **34**, 100383.
16 Y. Pan, C. Zhang, S. Yang, Y. Liu and A. Muhammad, *Nanotechnol. Rev.*, 2023, **12**, 20220530.
17 R. Hosny, A. Zahran, A. Abotaleb, M. Ramzi, M. F. Mubarak, M. A. Zayed, A. E. Shahawy and M. F. Hussein, *ACS Omega*, 2023, **8**, 46325–46345.
18 H. Farhangian, S. M. Abrishamifar, M. Palizian, M. J. Lariche and A. Baghban, *Pet. Sci. Technol.*, 2018, **36**, 287–292.
19 L. Hendraningrat and O. Torsaeter, *Appl. Nanosci.*, 2015, **5**, 181–199.
20 B. L. Peng, L. C. Zhang, J. H. Luo, P. M. Wang, B. Ding, M. X. Zeng and Z. D. Cheng, *RSC Adv.*, 2017, **7**, 32246–32254.
21 B. L. Peng, J. T. Tang, J. H. Luo, P. M. Wang, B. Ding and K. C. Tam, *Can. J. Chem. Eng.*, 2018, **96**, 91–100.
22 K. Jiang, C. Xiong, B. Ding, X. Geng, W. Liu, W. Chen, T. Huang, H. Xu, Q. Xu and B. Liang, *Energy Fuels*, 2023, **37**, 10045–10060.

23 Y. Ahmadi and S. M. A. Kariminia, *J. Mol. Liq.*, 2023, **390**, 123038.
24 M. S. Kamal, A. A. Adewunmi, A. S. Sultan, M. F. Al-Hamad and U. Mehmood, *J. Nanomater.*, 2017, **2017**, 2473175.
25 K. A. Hussain, C. Chen, R. Haggerty, M. Schubert and Y. S. Li, *Ind. Eng. Chem. Res.*, 2022, **61**, 17715–17734.
26 A. Keykhosravi, M. B. Vanani, A. Daryasafar and C. Aghayari, *J. Mol. Liq.*, 2021, **324**, 115093.
27 K. Wang, Q. You, Q.-M. Long, B. Zhou and P. Wang, *Pet. Sci.*, 2023, **20**, 382–395.
28 S. S. Ashrafmansouri and M. N. Esfahany, *Int. J. Therm. Sci.*, 2014, **82**, 84–99.
29 T. Liang, H. Wang and C. Yang, *J. Mol. Liq.*, 2024, **397**, 124043.
30 J. Zhao and D. S. Wen, *RSC Adv.*, 2017, **7**, 41391–41398.
31 A. Rahman, PhD thesis, The University of Regina, Canada, 2023.
32 S. Laibach, MSc thesis, State University of New York at Buffalo, 2023.
33 G. A. Manjangkarani Giridharan, MSc thesis, State University of New York at Buffalo, 2023.
34 M. B. Gawande, A. Goswami, F. X. Felpin, T. Asefa, X. X. Huang, R. Silva, X. X. Zou, R. Zboril and R. S. Varma, *Chem. Rev.*, 2016, **116**, 3722–3811.
35 A. Aziz, W. Jamshed, Y. Ali and M. Shams, *Discrete and Continuous Dynamical Systems-Series S*, 2020, 13, 2667–2690.
36 C. L. Zhang, L. C. Zheng, X. X. Zhang and G. Chen, *Appl. Math. Model.*, 2015, **39**, 165–181.
37 X. Z. Wang, Y. R. He, X. Liu, L. Shi and J. Q. Zhu, *Sol. Energy*, 2017, **157**, 35–46.
38 C. X. Wang, J. Yang and Y. L. Ding, *Prog. Nat. Sci.: Mater. Int.*, 2013, **23**, 338–342.
39 K. S. Hong, T. K. Hong and H. S. Yang, *Appl. Phys. Lett.*, 2006, **88**, 031901.
40 A. E. Bayat, R. Junin, A. Samsuri, A. Piroozian and M. Hokmabadi, *Energy Fuels*, 2014, **28**, 6255–6266.
41 S. Baek, D. Shin, G. Kim, A. Lee, J. Noh, B. Choi, S. Huh, H. Jeong and Y. M. Sung, *Case Stud. Therm. Eng.*, 2021, **25**, 100995.
42 A. Komeilibirjandi, A. H. Raffiee, A. Maleki, M. A. Nazari and M. S. Shadloo, *J. Therm. Anal. Calorim.*, 2020, **139**, 2679–2689.
43 M. Zarringhalam, A. Karimipour and D. Toghraie, *Exp. Therm. Fluid Sci.*, 2016, **76**, 342–351.
44 H. M. Ali, H. Babar, T. R. Shah, M. U. Sajid, M. A. Qasim and S. Javed, *Appl. Sci.*, 2018, **8**(4), 587.
45 L. Fedele, L. Colla and S. Bobbo, *Int. J. Refrig.*, 2012, **35**, 1359–1366.
46 A. Karimi, Z. Fakhroueian, A. Bahramian, N. P. Khiabani, J. B. Darabad, R. Azin and S. Arya, *Energy Fuels*, 2012, **26**, 1028–1036.
47 X. Wang, L. He, P. Xue, Y. Feng, Y. Huang and X. Wang, *Energy Fuels*, 2024, **38**, 7773–7785.
48 P. H. Shao, D. H. Liang, L. M. Yang, H. Shi, Z. S. Xiong, L. Ding, X. C. Yin, K. Zhang and X. B. Luo, *J. Hazard. Mater.*, 2020, **387**, 121676.
49 Z. Dong, L. Feng, Y. Hao, Q. Li, M. Chen, Z. Yang, H. Zhao and Z. Liu, *Chem*, 2020, **6**, 1391–1407.
50 A. Roustaei, S. Saffarzadeh and M. Mohammadi, *Egypt. J. Pet.*, 2013, **22**, 427–433.
51 C. R. Miranda, L. S. de Lara and B. C. Tonetto, *SPE International Oilfield Nanotechnology Conference and Exhibition*, 2012, All Days, SPE-157033-MS, DOI: **10.2118/157033-MS**.
52 T. Yousefi, E. Shojaeizadeh, F. Veysi and S. Zinadini, *Sol. Energy*, 2012, **86**, 771–779.
53 N. Domun, H. Hadavinia, T. Zhang, T. Sainsbury, G. H. Liaghat and S. Vahid, *Nanoscale*, 2015, **7**, 10294–10329.
54 K. A. P. Chandran, *Universiti Teknologi PETRONAS*, 2013.
55 K. Guo, H. L. Li and Z. X. Yu, *Fuel*, 2016, **185**, 886–902.
56 M. Schneider, S. M. de Amorim, K. Cesca, J. da Silveira Salla, D. Hotza, E. Rodriguez-Castellon, R. A. Peralta and R. F. P. M. Moreira, *J. Mol. Liq.*, 2023, **390**, 123097.
57 X. Ma, H. Yang, X. Liu, L. Zeng, X. Li, L. Zheng, Y. Yang, L. Cao, W. Meng and J. Zheng, *Polymers*, 2024, **16**(8), 1085.
58 Y. Mao, A. L. Lanzon, B. Zheng, Z. Xu, J. Jiang, D. Harbottle, K. Yu, M. Chen, Y. Sheng and H. Zhang, *Polymers*, 2023, **15**(11), 2515.
59 H. Shen, Z.-H. Yang, G.-Z. Wang, Y.-L. Xiong, Q.-C. Lv, Q. Cao, Q.-Q. Niu, Y.-B. Wang and Z.-X. Dong, *Pet. Sci.*, 2023, **20**, 1584–1597.
60 K. R. Chaturvedi and T. Sharma, *Mater. Today: Proc.*, 2021, **46**, 5298–5303.
61 W. Sun, H. Pu, D. Pierce and J. X. Zhao, *Energy Fuels*, 2023, **37**, 16267–16281.
62 K. Abe, K. Negishi and H. Fujii, *Energy Fuels*, 2023, **37**, 7122–7129.
63 J. Zhang, H. Huang, M. Zhang and W. Wang, *RSC Adv.*, 2023, **13**, 16165–16174.
64 R. Fattahi, M. Lashkarbolooki, R. Abedini and H. Younesi, *Energy Fuels*, 2023, **37**, 14741–14751.
65 K. Raghav Chaturvedi, R. Kumar, J. Trivedi, J. J. Sheng and T. Sharma, *Energy Fuels*, 2018, **32**, 12730–12741.
66 K. R. Chaturvedi, J. Trivedi and T. Sharma, *Energy*, 2020, **197**, 117276.
67 K. Y. Leong, R. Saidur, M. Khairulmaini, Z. Michael and A. Kamyar, *Int. Commun. Heat Mass Transfer*, 2012, **39**, 838–843.
68 M. Parsazadeh, H. A. Mohammed and F. Fathinia, *Int. Commun. Heat Mass Transfer*, 2013, **46**, 97–105.
69 A. M. Rashad, M. M. Rashidi, G. Lorenzini, S. E. Ahmed and A. M. Aly, *Int. J. Heat Mass Transfer*, 2017, **104**, 878–889.
70 M. Sheikholeslami, M. Gorji-Bandpay and D. D. Ganji, *Int. Commun. Heat Mass Transfer*, 2012, **39**, 978–986.
71 M. T. Jamal-Abad, A. Zamzamian, E. Imani and M. Mansouri, *J. Thermophys. Heat Transfer*, 2013, **27**, 756–760.
72 I. M. Mahbubul, E. B. Elcioglu, R. Saidur and M. A. Amalina, *Ultrason. Sonochem.*, 2017, **37**, 360–367.
73 Y. R. Sekhar and K. V. Sharma, *J. Exp. Nanosci.*, 2015, **10**, 86–102.

74 T. P. Teng and Y. H. Hung, *J. Exp. Nanosci.*, 2014, **9**, 707–718.
75 S. Aberoumand and A. Jafarimoghaddam, *J. Taiwan Inst. Chem. Eng.*, 2017, **71**, 315–322.
76 H. A. Mohammed, A. A. Al-Aswadi, N. H. Shuaib and R. Saidur, *Renewable Sustainable Energy Rev.*, 2011, **15**, 2921–2939.
77 W. H. Fan and F. Q. Zhong, *Thermochim. Acta*, 2022, **712**, 179229.
78 M. B. Xing, J. L. Yu and R. X. Wang, *Int. J. Heat Mass Transfer*, 2015, **88**, 609–616.
79 A. A. Minea, *Curr. Nanosci.*, 2013, **9**, 81–88.
80 A. Kaushik, D. Joshi, R. K. Saw, K. B. Rathi, S. Mitra and A. Mandal, *Fuel*, 2024, **359**, 130500.
81 C. Y. Zhang, M. Oostrom, T. W. Wietsma, J. W. Grate and M. G. Warner, *Energy Fuels*, 2011, **25**, 3493–3505.
82 K. Sefiane, J. Skilling and J. MacGillivray, *Adv. Colloid Interface Sci.*, 2008, **138**, 101–120.
83 E. Joonaki and S. Ghanaatian, *Pet. Sci. Technol.*, 2014, **32**, 2599–2607.
84 Z. Tohidi, A. Jafari and M. Omidkhah, *Korean J. Chem. Eng.*, 2024, **41**, 1077–1092.
85 H. Ma, M. X. Luo and L. L. Dai, *Phys. Chem. Chem. Phys.*, 2008, **10**, 2207–2213.
86 B. Moradi, P. Pourafshary, F. Jalali, M. Mohammadi and M. A. Emadi, *J. Nat. Gas Sci. Eng.*, 2015, **27**, 64–73.
87 A. Maghzi, S. Mohammadi, M. H. Ghazanfari, R. Kharrat and M. Masihi, *Exp. Therm. Fluid Sci.*, 2012, **40**, 168–176.
88 L. O. Boampong, R. Rafati and A. S. Haddad, *Fuel*, 2023, **331**, 125856.
89 T. Sharma, S. Iglauer and J. S. Sangwai, *Ind. Eng. Chem. Res.*, 2016, **55**, 12387–12397.
90 S. Al-Anssari, M. Arif, S. Wang, A. Barifcani and S. Iglauer, *J. Colloid Interface Sci.*, 2017, **508**, 222–229.
91 S. Ahualli, G. R. Iglesias, W. Wachter, M. Dulle, D. Minami and O. Glatter, *Langmuir*, 2011, **27**, 9182–9192.
92 R. S. Kumar, K. R. Chaturvedi, S. Iglauer, J. Trivedi and T. Sharma, *J. Pet. Sci. Eng.*, 2020, **195**, 107634.
93 K. R. Chaturvedi and T. Sharma, *J. Pet. Sci. Eng.*, 2021, **196**, 107704.
94 P. Pillai, R. K. Saw, R. Singh, E. Padmanabhan and A. Mandal, *J. Pet. Sci. Eng.*, 2019, **177**, 861–871.
95 L. M. Corredor, M. M. Husein and B. B. Maini, *Ind. Eng. Chem. Res.*, 2019, **58**, 9888–9899.
96 R. K. Saw, A. Singh, N. K. Maurya and A. Mandal, *Colloids Surf., A*, 2023, **666**, 131308.
97 N. Pal, N. Kumar, R. K. Saw and A. Mandal, *J. Pet. Sci. Eng.*, 2019, **183**, 106464.
98 M. K. Chaudhury, *Nature*, 2003, **423**, 131–132.
99 D. T. Wasan and A. D. Nikolov, *Nature*, 2003, **423**, 156–159.
100 H. Zhang, A. Nikolov and D. Wasan, *Energy Fuels*, 2014, **28**, 3002–3009.
101 P. X. Cui, W. W. Liang and B. C. Hou, *Unconv. Oil Gas Resour.: Exploit. Dev.*, 2021, **8**, 66.
102 P. C. Myint and A. Firoozabadi, *Curr. Opin. Colloid Interface Sci.*, 2015, **20**, 105–114.
103 R. A. Nasralla and H. A. Nasr-El-Din, *SPE Asia Pacific Oil and Gas Conference and Exhibition*, 2011, All Days, SPE-147937-MS, DOI: **10.2118/147937-MS**.
104 U. Farooq, M. T. Tweheyo, J. Sjöblom and G. Oye, *J. Dispersion Sci. Technol.*, 2011, **32**, 519–531.
105 K. Kondiparty, A. D. Nikolov, D. Wasan and K. L. Liu, *Langmuir*, 2012, **28**, 14618–14623.
106 Y. Y. Li, C. L. Dai, H. D. Zhou, X. K. Wang, W. J. Lv and M. W. Zhao, *Energy Fuels*, 2018, **32**, 287–293.
107 D. Wasan, A. Nikolov and K. Kondiparty, *Curr. Opin. Colloid Interface Sci.*, 2011, **16**, 344–349.
108 S. Wu, A. Nikolov and D. Wasan, *J. Colloid Interface Sci.*, 2013, **396**, 293–306.
109 V. Bergeron, *Doctoral*, University of California, Berkeley, 1993.
110 T. D. Dimitrova, F. Leal-Calderon, T. D. Gurkov and B. Campbell, *Langmuir*, 2001, **17**, 8069–8077.
111 T. D. Dimitrova, F. Leal-Calderon, T. D. Gurkov and B. Campbell, *Adv. Colloid Interface Sci.*, 2004, **108**, 73–86.
112 A. Zou, S. Poudel, M. Gupta and S. C. Maroo, *Nano Lett.*, 2021, **21**, 7769–7774.
113 L. G. C. Pereira, C. Johansson, C. J. Radke and H. W. Blanch, *Langmuir*, 2003, **19**, 7503–7513.
114 T. D. Dimitrova and F. Leal-Calderon, *Adv. Colloid Interface Sci.*, 2004, **108**, 49–61.
115 A. Nikolov, K. Kondiparty and D. Wasan, *Langmuir*, 2010, **26**, 7665–7670.
116 Y. Ma, M. Sun, X. X. Duan, A. van den Berg, J. C. T. Eijkel and Y. B. Xie, *Nat. Commun.*, 2020, **11**, 814.
117 S. I. Karakashev, A. V. Nguyen and E. D. Manev, *J. Colloid Interface Sci.*, 2007, **306**, 449–453.